Available online at www.sciencedirect.com
SCIENCE DIRECT®
Journal of Solid State Chemistry 176 (2003) 5–12
JOURNAL OF SOLID STATE CHEMISTRY
http://elsevier.com/locate/jssc

Syntheses, structures, physical properties, and electronic structures of KLn_2CuS_4 (Ln = Y, Nd, Sm, Tb, Ho) and $K_2Ln_4Cu_4S_9$ (Ln = Dy, Ho)

Jiyong Yao,[a] Bin Deng,[a] Donald E. Ellis,[a,b] and James A. Ibers[a,*]

[a] *Department of Chemistry, Northwestern University, 2145 Sheridan Road, Evanston, IL 60208-3113, USA*
[b] *Department of Physics and Astronomy, Northwestern University, 2145 Sheridan Road, Evanston, IL 60208-3113, USA*

Received 2 January 2003; received in revised form 14 April 2003; accepted 25 April 2003

Abstract

Seven new quaternary metal sulfides, KY_2CuS_4, KNd_2CuS_4, KSm_2CuS_4, KTb_2CuS_4, KHo_2CuS_4, $K_2Dy_4Cu_4S_9$, and $K_2Ho_4Cu_4S_9$, were prepared by the reactive flux method. All crystallographic data were collected at 153 K. The isostructural compounds KLn_2CuS_4 (Ln = Y, Nd, Sm, Tb, Ho) crystallize in space group *Cmcm* of the orthorhombic system with four formula units in cells of dimensions (Ln, a, b, c (Å)): Y, 3.9475(9), 13.345(3), 13.668(3); Nd, 4.0577(3), 13.7442(10), 13.9265(10); Sm, 4.0218(4), 13.6074(14), 13.8264(14); Tb, 3.9679(5), 13.4243(17), 13.7102(18); Ho, 3.9378(3), 13.3330(11), 13.6487(11). The corresponding R_1 indices for the refined structures are 0.0197, 0.0153, 0.0158, 0.0181, and 0.0178. The isostructural compounds $K_2Dy_4Cu_4S_9$ and $K_2Ho_4Cu_4S_9$ crystallize in space group $C2/m$ of the monoclinic system with two formula units in cells of dimensions (Ln, a, b, c (Å), β (°)): Dy, 13.7061(13), 3.9482(4), 15.8111(15), 109.723(1); Ho, 13.6760(14), 3.9360(4), 15.7950 (16), 109.666(2). The corresponding R_1 indices are 0.0312 and 0.0207. Both structure types are closely related three-dimensional tunnel structures. The tunnels are filled with bicapped trigonal-prismatically coordinated K atoms. Their anionic frameworks are built from LnS_6 octahedra and CuS_4 tetrahedra. KLn_2CuS_4 contains $^1_\infty[CuS_3^{5-}]$ chains of vertex-sharing tetrahedra and $K_2Ln_4Cu_4S_9$ contains $^1_\infty[Cu_4S_8^{12-}]$ chains of tetrahedra. $K_2Ho_4Cu_4S_9$ shows Curie–Weiss paramagnetic behavior between 5 and 300 K, and has an effective magnetic moment of 10.71 μ_B for Ho^{3+} at 293 K. Optical band gaps of 2.17 eV for KSm_2CuS_4 and 2.43 eV for $K_2Ho_4Cu_4S_9$ were deduced from diffuse reflectance spectra. A first-principles calculation of the density of states and the frequency-dependent optical conductivity was performed on KSm_2CuS_4. The calculated band gap of 2.1 eV is in good agreement with the experimental value.

1. Introduction

Ternary and quaternary chalcogenides containing a combination of *d*- and *f*-elements have been reviewed recently [1]. These compounds are of interest in solid-state chemistry and materials science because of their physical properties and their rich structural chemistry.

Quaternary phases containing an alkali metal, in addition to the chalcogen and the 3*d* and 4*f* metals, are generally conveniently prepared by the reactive flux technique [2]. Here we report the syntheses, structures, physical properties, and electronic structures of seven new compounds containing *f*- and *d*-block metals, namely the quaternary compounds KLn_2CuS_4 (Ln = Y, Nd, Sm, Tb, Ho) and $K_2Ln_4Cu_4S_9$ (Ln = Dy, Ho). These compounds comprise four elements with different coordination preferences [3] and thus are free of crystallographic disorder.

2. Experimental

2.1. Syntheses

The following reagents were used as obtained: K (Aldrich, 98 + %), Y (Alfa, 99.9%), Nd (Alfa, 99.9%), Sm (Alfa, 99.9%), Tb (Alfa, 99.9%), Dy (Strem, 99.9%), Ho (Alfa, 99.9%), Cu (Aldrich, 99.999%), S (Aldrich, 99.5%). K_2S, the reactive flux [2] employed in the syntheses, was prepared by the stoichiometric reaction of the elements in liquid NH_3. For the syntheses of KLn_2CuS_4 (Ln = Y, Nd, Sm) and $K_2Ln_4Cu_4S_9$ (Ln = Dy, Ho), the starting materials were 0.6 mmol K_2S, 0.5 mmol Ln, 0.5 mmol Cu, 2.7 mmol S, and 66 mg

*Corresponding author. Department of Chemistry, Northwestern University, 2145 Sheridan Road, Evanston, IL 60208-3113, USA. Fax: +1-847-491-2976.
E-mail address: ibers@chem.northwestern.edu (J.A. Ibers).

0022-4596/03/$ - see front matter © 2003 Elsevier Inc. All rights reserved.
doi:10.1016/S0022-4596(03)00233-0

KI (added to aid crystal growth); for the syntheses of KTb_2CuS_4 and KHo_2CuS_4, the starting materials were 1.2 mmol K_2S, 1.0 mmol *Ln*, 0.5 mmol Cu, 4.4 mmol S, and 132 mg KI. The reactants were loaded into fused-silica tubes under an Ar atmosphere in a glove box. These tubes were sealed under a 10^{-4} Torr atmosphere and then placed in a computer-controlled furnace. The samples were heated to 523 K in 15 h, kept at 523 K for 10 h, then heated to 973 K in 15 h, kept at 973 K for 4 days, slowly cooled at 5 K/h to 373 K, and then cooled to room temperature. The reaction mixtures were washed free of flux with water and dried with acetone. Major products were orange-red (KNd_2CuS_4 and KSm_2CuS_4), yellow (KTb_2CuS_4, KHo_2CuS_4, $K_2Dy_4Cu_4S_9$, and $K_2Ho_4Cu_4S_9$), or green (KY_2CuS_4) needles of the titled materials. Yields varied from 40% to 90% based on *Ln*. Analyses of these compounds with an EDX-equipped Hitachi S-3500 SEM showed the presence of K, *Ln*, Cu, and S but no I. All these compounds are modestly stable in air.

2.2. Crystallography

Single-crystal X-ray diffraction data were obtained with the use of graphite-monochromatized Mo$K\alpha$ radiation ($\lambda = 0.71073$ Å) at 153 K on a Bruker Smart-1000 CCD diffractometer [4]. The crystal-to-detector distance was 5.023 cm. Crystal decay was monitored by re-collecting 50 initial frames at the end of data collection. Data were collected by a scan of 0.3° in ω in groups of 606, 606, 606, and 606 frames at ϕ settings of 0°, 90°, 180°, and 270° for all the compounds except $K_2Ho_4Cu_4S_9$, for which 606, 606, and 606 frames at φ settings of 0°, 120°, and 240° were collected. The exposure times varied from 10 to 20 s/frame. The collection of intensity data was carried out with the program SMART [4]. Cell refinement and data reduction were carried out with the use of the program SAINT [4] and face-indexed absorption corrections were carried out numerically with the program XPREP [5]. The program SADABS [4] was employed to make incident beam and decay corrections.

The structures were solved with the direct methods program SHELXS and refined with the full-matrix least-squares program SHELXL of the SHELXTL-PC suite of programs [5]. Each final refinement included anisotropic displacement parameters. A secondary extinction correction was included for each KLn_2CuS_4 compound. The program TIDY [6] was then employed to standardize the atomic coordinates in each structure. Additional crystallographic details are given in Table 1. Tables 2 and 3 give positional parameters and equivalent isotropic displacement parameters, and Tables 4 and 5 present selected bond distances for KLn_2CuS_4 (*Ln* = Y, Nd, Sm, Tb, Ho) and $K_2Ln_4Cu_4S_9$ (*Ln* = Dy, Ho).

2.3. Magnetic susceptibility measurement

Magnetic susceptibility as a function of temperature was measured on a 35.0 mg sample of $K_2Ho_4Cu_4S_9$ with the use of a Quantum Design SQUID magnetometer (MPMSS Quantum Design). The sample was loaded into a gelatin capsule. Zero-field cooled (ZFC) susceptibility data were collected between 5 and 300 K at an applied field of 500 G. The susceptibility data in the temperature range 5–300 K were fit by a least-squares procedure to the Curie–Weiss equation $\chi = C/(T - \theta_p)$, where C is the Curie constant and θ_p is the Weiss constant. The effective moment (μ_{eff}) was calculated from the equation $\mu_{eff} = (7.997C)^{1/2}\mu_B$ [7].

Table 1
Crystal data and structure refinement for KLn_2CuS_4 and $K_2Ln_4Cu_4S_9$[a]

Compound	KY_2CuS_4	KNd_2CuS_4	KSm_2CuS_4	KTb_2CuS_4	KHo_2CuS_4	$K_2Dy_4Cu_4S_9$	$K_2Ho_4Cu_4S_9$
Formula weight	408.70	519.36	531.58	548.72	560.74	1270.90	1280.62
a (Å)	3.9475(9)	4.0577(3)	4.0218(4)	3.9679(5)	3.9378(3)	13.7061(13)	13.6760(14)
b (Å)	13.345(3)	13.7442(10)	13.6074(14)	13.4243(17)	13.3330(11)	3.9482(4)	3.9360(4)
c (Å)	13.668(3)	13.9265(10)	13.8264(14)	13.7102(18)	13.6487(11)	15.8111(15)	15.7950(16)
β (Å)	90	90	90	90	90	109.723(1)	109.666(2)
V (Å^3)	720.0 (3)	776.68(10)	756.67(13)	730.29(16)	716.59(10)	805.41(14)	800.63(14)
Space group	*Cmcm*	*Cmcm*	*Cmcm*	*Cmcm*	*Cmcm*	*C*2/*m*	*C*2/*m*
Z	4	4	4	4	4	2	2
ρ_c (g/cm^3)	3.770	4.442	4.666	4.991	5.198	5.240	5.312
μ (cm^{-1})	205.32	173.86	196.43	236.39	264.35	251.32	263.81
$R(F)$[b]	0.0197	0.0153	0.0158	0.0181	0.0178	0.0312	0.0207
$R_w(F_o^2)$[c]	0.0456	0.0431	0.0407	0.0437	0.0433	0.0885	0.0508

[a] For all structures $T = 153(2)$ K, and $\lambda = 0.71073$ Å.
[b] $R(F) = \sum||F_o| - |F_c||/\sum|F_o|$ for $F_o^2 > 2\sigma(F_o^2)$.
[c] $R_w(F_o^2) = \{\sum[w(F_o^2 - F_c^2)^2]/\sum wF_o^4\}^{1/2}$ for all data. $w^{-1} = \sigma^2(F_o^2) + (z \times P)^2$, where $P = (\mathrm{Max}(F_o^2, 0) + 2F_c^2)/3$; $z = 0.02$ for KLn_2CuS_4 and $K_2Ho_4Cu_4S_9$, and 0.03 for $K_2Dy_4Cu_4S_9$.

Table 2
Atomic coordinates[a] and equivalent isotropic displacement parameters (Å^2) for KY_2CuS_4, KNd_2CuS_4, KSm_2CuS_4, KTb_2CuS_4, and KHo_2CuS_4

Atom	y	z	U_{eq}[b]
KY_2CuS_4			
K	0.11015(7)	1/4	0.0102(2)
Y	0.36578(2)	0.063151(18)	0.0048(1)
Cu	0.83744(4)	1/4	0.0076(2)
S1	0.43252(8)	1/4	0.0057(2)
S2	0.26425(5)	0.61065(5)	0.0059(2)
S3	0	0	0.0076(2)
KNd_2CuS_4			
K	0.10787(8)	1/4	0.0116(2)
Nd	0.365717(13)	0.062444(13)	0.0052(1)
Cu	0.83757(5)	1/4	0.0081(2)
S1	0.43118(9)	1/4	0.0057(2)
S2	0.26365(6)	0.61373(6)	0.0065(2)
S3	0	0	0.0086(2)
KSm_2CuS_4			
K	0.10861(8)	1/4	0.0115(2)
Sm	0.365805(12)	0.062544(12)	0.0054(1)
Cu	0.83785(5)	1/4	0.0082(2)
S1	0.43168(9)	1/4	0.0060(2)
S2	0.26364(6)	0.61268(6)	0.0064(2)
S3	0	0	0.0085(2)
KTb_2CuS_4			
K	0.10950(12)	1/4	0.0108(3)
Tb	0.365869(17)	0.062906(15)	0.0054(1)
Cu	0.83765(7)	1/4	0.0080(2)
S1	0.43253(13)	1/4	0.0057(3)
S2	0.26412(9)	0.61114(9)	0.0066(2)
S3	0	0	0.0078(3)
KHo_2CuS_4			
K	0.10995(12)	1/4	0.0105(3)
Ho	0.365900(16)	0.063193(15)	0.0053(1)
Cu	0.83730(7)	1/4	0.0078(2)
S1	0.43255(13)	1/4	0.0058(3)
S2	0.26409(9)	0.61017(9)	0.0061(2)
S3	0	0	0.0078(3)

[a] The x coordinate of all atoms is 0.
[b] U_{eq} is defined as one-third of the trace of the orthogonalized U_{ij} tensor.

Table 3
Atomic coordinates[a] and equivalent isotropic displacement parameters (Å^2) for $K_2Dy_4Cu_4S_9$ and $K_2Ho_4Cu_4S_9$

Atom	x	z	U_{eq}
$K_2Dy_4Cu_4S_9$			
K	0.02819(18)	0.76918(16)	0.0120(5)
Dy1	0.65433(3)	0.05356(3)	0.0061(2)
Dy2	0.23313(3)	0.60508(3)	0.0059(2)
Cu1	0.24655(10)	0.22894(8)	0.0091(3)
Cu2	0.43211(10)	0.54063(9)	0.0105(3)
S1	0.1388(2)	0.42449(16)	0.0065(5)
S2	0.30065(18)	0.10273(16)	0.0061(5)
S3	0.39047(18)	0.37268(16)	0.0064(5)
S4	0.6494(2)	0.22101(16)	0.0076(5)
S5	0	0	0.0087(7)
$K_2Ho_4Cu_4S_9$			
K	0.02912(11)	0.76952(10)	0.0163(3)
Ho1	0.65436(2)	0.054038(17)	0.00779(9)
Ho2	0.23340(2)	0.605250(18)	0.00770(9)
Cu1	0.24616(7)	0.22889(5)	0.0137(2)
Cu2	0.43268(6)	0.54175(6)	0.0162(2)
S1	0.13991(12)	0.42452(10)	0.0080(3)
S2	0.29974(11)	0.10224(10)	0.0079(3)
S3	0.38927(11)	0.37266(10)	0.0084(3)
S4	0.64929(12)	0.22106(10)	0.0096(3)
S5	0	0	0.0115(4)

[a] The y coordinate of all atoms is 0.

2.4. UV–visible diffuse reflectance spectroscopy

A Cary 1E UV–visible spectrophotometer with a diffuse reflectance accessory was used to measure the diffuse reflectance spectra of the compounds KSm_2CuS_4 and $K_2Ho_4Cu_4S_9$ over the range 350 nm (3.54 eV)–850 nm (1.46 eV) at 293 K.

2.5. Theoretical calculations

Calculations for KSm_2CuS_4 were performed by means of the FP-LAPW method [8,9], as implemented in the WIEN2k code [10]; included were local orbitals for high-lying semicore states. The exchange correlations were treated in the local density approximation (LDA) within density-functional theory by parametrization [11]. The muffin-tin radii were 2.8, 2.8, 2.3, and 2.1 bohr for K, Sm, Cu, and S, respectively. The K_{max} and G_{max} values, which are the plane-wave expansion cutoffs for wave functions and for the densities and potentials, respectively, were chosen as 7 and 14. Open-core treatment was performed on 4f electrons in order to overcome the shortcomings of the LDA. LDA always puts the 4f states around the Fermi energy and yields a fractional occupation. In the present open-core treatment, the potential was shifted by a constant. The resulting eigenvalues were also shifted by this same constant. The electron density was not affected by this procedure. Although this open-core treatment eliminates the problem of 4f states around the Fermi energy level, it does not allow the study of the optical transitions related to the 4f states. Brillouin-zone integrations with self-consistency cycles were performed by means of a tetrahedron method [12] with the use of 42 inequivalent k points corresponding to 200 k points throughout the Brillouin zone. For the calculation of the optical properties, a denser sampling of the Brillouin zone of 86 inequivalent k points corresponding to 600 k points throughout the Brillouin zone was used. The frequency-dependent optical properties were obtained with the use of the joint density of states (JDOS) weighted by the dipole matrix elements of the optical

Table 4
Selected distances (Å) for KY_2CuS_4, KNd_2CuS_4, KSm_2CuS_4, KTb_2CuS_4, and KHo_2CuS_4

	KY_2CuS_4	KNd_2CuS_4	KSm_2CuS_4	KTb_2CuS_4	KHo_2CuS_4
K–S1 × 2	3.085(1)	3.164(1)	3.137(1)	3.095(2)	3.078(2)
K–S2 × 4	3.2144(9)	3.2918(9)	3.2665(9)	3.231(1)	3.216(1)
K–S3 × 2	3.7198(8)	3.7841(5)	3.7593(6)	3.7294(8)	3.7137(7)
Ln–S1	2.7048(7)	2.7626(5)	2.7425(5)	2.7167(7)	2.7001(7)
Ln–S2 × 2	2.7070(7)	2.7907(6)	2.7617(6)	2.7237(8)	2.7002(8)
Ln–S2	2.7348(9)	2.8262(9)	2.7932(8)	2.750(1)	2.728(1)
Ln–S3 × 2	2.8016(5)	2.8773(2)	2.8506(2)	2.8146(3)	2.7959(2)
Cu–S1 × 2	2.3464(8)	2.4025(8)	2.3820(8)	2.358(1)	2.343(1)
Cu–S2 × 2	2.3386(9)	2.3530(9)	2.3478(9)	2.343(1)	2.339(1)

Table 5
Selected distances (Å) for $K_2Dy_4Cu_4S_9$ and $K_2Ho_4Cu_4S_9$

	$K_2Dy_4Cu_4S_9$	$K_2Ho_4Cu_4S_9$
K–S1	3.144(3)	3.157(2)
K–S2 × 2	3.209(3)	3.204(2)
K–S3 × 2	3.444(3)	3.442(2)
K–S4 × 2	3.178(3)	3.177(2)
K–S5	3.797(2)	3.793(2)
*Ln*1–S2 × 2	2.733(2)	2.718(1)
*Ln*1–S2	2.742(2)	2.744(2)
*Ln*1–S4	2.671(3)	2.662(2)
*Ln*1–S5 × 2	2.8071(4)	2.8009(3)
*Ln*2–S1	2.708(2)	2.707(2)
*Ln*2–S1 × 2	2.784(2)	2.765(1)
*Ln*2–S3 × 2	2.701(2)	2.684(1)
*Ln*2–S4	2.677(2)	2.672(2)
Cu1–S2	2.352(3)	2.351(2)
Cu1–S3	2.456(3)	2.449(2)
Cu1–S4 × 2	2.361(2)	2.352(1)
Cu2–S1 × 2	2.347(2)	2.3448(9)
Cu2–S3	2.354(3)	2.354(2)
Cu2–S3	2.521(3)	2.534(2)

transitions [13]. Since the diffuse reflectance spectrum was measured on powder samples, we also present an average over the three components, $(\sigma_{xx}+\sigma_{yy}+\sigma_{zz})/3$ [14].

3. Results and discussion

3.1. Syntheses

The quaternary metal sulfides KY_2CuS_4, KNd_2CuS_4, KSm_2CuS_4, KTb_2CuS_4, KHo_2CuS_4, $K_2Dy_4Cu_4S_9$, and $K_2Ho_4Cu_4S_9$ were prepared by the reactions of *Ln* and Cu with a K_2S/S reactive flux [2] at 973 K. KI was added to aid crystal growth. These compounds could be synthesized in the absence of KI, but the yields were lower. Efforts to synthesize the Na analogues were unsuccessful, presumably because the Na^+ cation is too small to sustain the anionic frameworks in these structures.

3.2. Structures

The isostructural compounds KLn_2CuS_4 crystallize in space group *Cmcm* of the orthorhombic system. In the asymmetric unit there is one crystallographically unique K atom at a site with *mm* symmetry, one unique *Ln* atom at a site with *m* symmetry, and one unique Cu atom at a site with *mm* symmetry. $K_2Ln_4Cu_4S_9$ crystallizes in space group $C2/m$ of the monoclinic system. There are five crystallographically unique metal sites with *m* symmetry (one K atom, two *Ln* atoms, and two Cu atoms) in the asymmetric unit. In all these compounds, the K atoms are coordinated to a bicapped trigonal prism of eight S atoms, the *Ln* atoms are coordinated to an octahedron of six S atoms, and the Cu atoms are coordinated to a tetrahedron of four S atoms. The shortest S–S distance in any of the seven compounds is 3.632(1) Å in KY_2CuS_4. Thus, there are no S–S bonds and oxidation states of 1+, 3+, 1+, and 2− can be assigned to K, *Ln*, Cu, and S, respectively.

The structure of KLn_2CuS_4 is shown in Fig. 1. This is the KGd_2CuS_4 structure type [15]. The structure of $K_2Ln_4Cu_4S_9$ is shown in Fig. 2. This is the $Rb_2Gd_4Cu_4S_9$ structure type [16]. Both structures possess three-dimensional tunnel frameworks with similarly shaped tunnels. Each tunnel is only large enough in cross section to accommodate one K atom. The tunnel in KLn_2CuS_4 consists of a 10-membered ring of two Cu–S bonds and eight *Ln*–S bonds, and that in $K_2Ln_4Cu_4S_9$ comprises a 10-membered ring of four Cu–S bonds and six *Ln*–S bonds.

The three-dimensional anionic frameworks in these structures are built up from LnS_6 octahedra and CuS_4 tetrahedra, as shown in Figs. 1 and 2. The *Ln*/S fragments in these structures are shown in Figs. 3 and 4. They consist of similar ${}^2_\infty[Ln_2S_5^{4-}]$ layers. As an example, the structure of this ${}^2_\infty[Ln_2S_5^{4-}]$ layer in KLn_2CuS_4 is shown in Fig. 5. There are ${}^1_\infty[Ln_2S_6^{6-}]$ chains along the [100] direction made up of edge-sharing LnS_6 octahedra. These chains are connected to each other by corner-sharing of S atoms to form a two-dimensional ${}^2_\infty[Ln_2S_5^{4-}]$ layer. This ${}^2_\infty[Ln_2S_5^{4-}]$ layer in

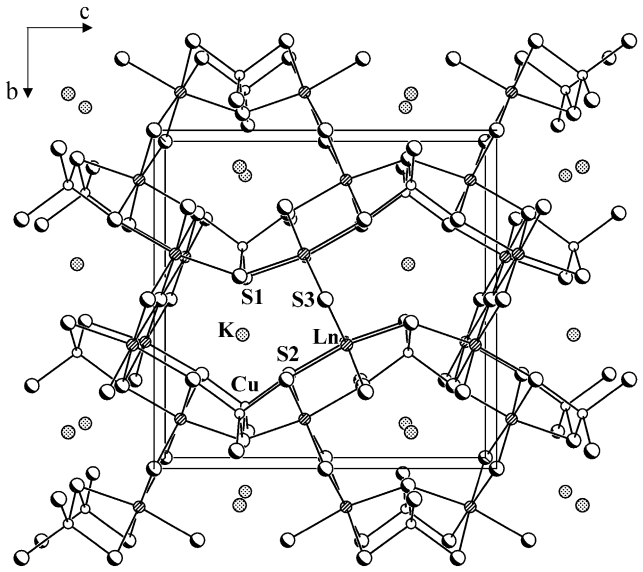

Fig. 1. Structure of KLn_2CuS_4 viewed down [100].

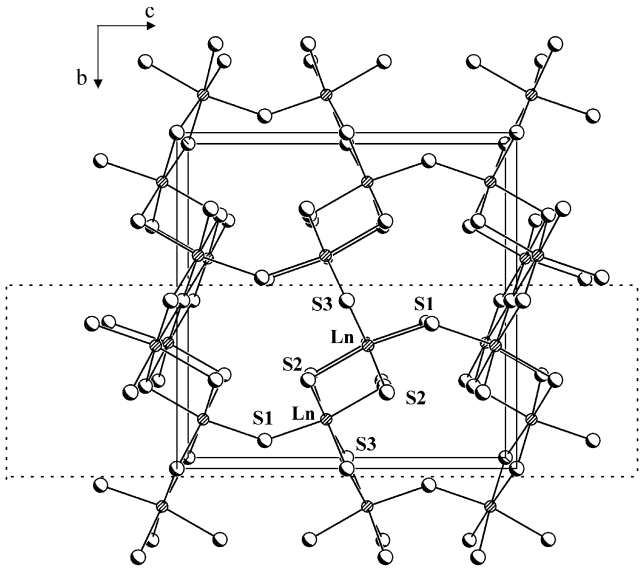

Fig. 3. The *Ln*/S fragment of KLn_2CuS_4 viewed down [100]. The $^{2}_{\infty}[Ln_2S_5^{4-}]$layer is in the dashed box.

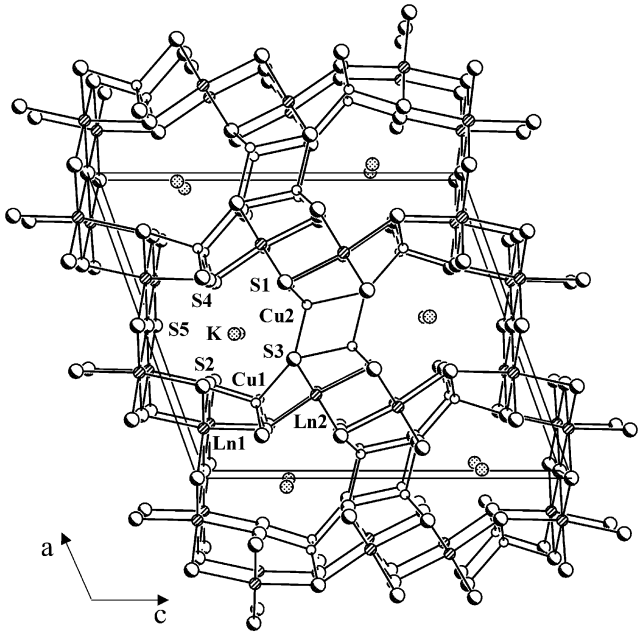

Fig. 2. Structure of $K_2Ln_4Cu_4S_9$ viewed down [010].

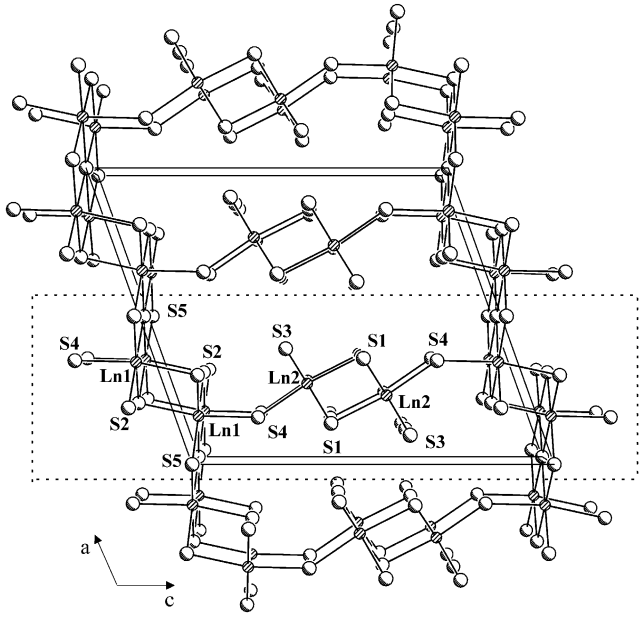

Fig. 4. The *Ln*/S fragment of $K_2Ln_4Cu_4S_9$ viewed down [010]. The $^{1}_{\infty}[Ln_2S_5^{4-}]$ layer is in the dashed box.

KLn_2CuS_4 and in $K_2Ln_4Cu_4S_9$ is connected to its neighboring layers by edge-sharing of two S atoms to form a three-dimensional framework. There is one crystallographically independent *Ln* atom and one unique $^{1}_{\infty}[Ln_2S_6^{6-}]$ chain in KLn_2CuS_4, but in $K_2Ln_4Cu_4S_9$ there are two crystallographically independent *Ln* atoms (*Ln*1, *Ln*2) and two chains ($^{1}_{\infty}[Ln1_2S_6^{6-}]$, $^{1}_{\infty}[Ln2_2S_6^{6-}]$). Each $^{1}_{\infty}[Ln_2S_6^{6-}]$ chain in KLn_2CuS_4 is connected to two chains in the neighboring layers by edge-sharing, whereas in $K_2Ln_4Cu_4S_9$ only $^{1}_{\infty}[Ln1_2S_6^{6-}]$ chain is connected to other layers.

In KLn_2CuS_4 there is one crystallographically unique Cu atom. The CuS_4 tetrahedra form a one-dimensional $^{1}_{\infty}[CuS_3^{5-}]$ chain along the [100] direction by corner-sharing (Fig. 6). In $K_2Ln_4Cu_4S_9$ there are two crystallographically unique Cu atoms (Cu1, Cu2). The structure contains one-dimensional $^{1}_{\infty}[Cu_4S_8^{12-}]$ chains made up of two $^{1}_{\infty}[Cu1S_3^{5-}]$ single chains and one $^{1}_{\infty}[Cu2_2S_4^{6-}]$ double chain (Fig. 7).

Selected bond distances for these seven compounds are listed in Tables 4 and 5. These bond lengths are

normal. The ranges of distances are: Y–S, 2.7048(7)–2.8016(5) Å; Nd–S, 2.7626(5)–2.8773(2) Å; Sm–S, 2.7425(5)–2.8506(2) Å; Tb–S, 2.7167(7)–2.8146(3) Å; Ho–S, 2.662(2)–2.8009(3) Å; Dy–S, 2.671(3)–2.8071(4) Å; and Cu–S, 2.3386(9)–2.534(3) Å. These ranges are consistent, for example, with those of 2.670(1)–2.792(1) Å for Y–S in $K_2Y_4Sn_2S_{11}$ [17]; 2.7622(7)–2.8976(2) Å for Nd–S in $RbNd_2CuS_4$ [18]; 2.7394(6)–2.8704(2) Å for Sm–S in $RbSm_2CuS_4$ [18]; 2.752(4)–2.831(4) Å for Tb–S in $Ba_4Tb_2Cd_3S_{10}$ [19]; 2.719(2)–3.057(3) Å for Dy–S in Dy_2S_3 (α-Gd_2S_3 structure type) [20]; 2.649(8)–2.768(8) Å for Ho–S in $AgHoS_2$ [21]; and 2.369(2)–2.549(1) Å for Cu–S in $Rb_2Gd_4Cu_4S_9$ [18], respectively. The shortest K–S distance of 3.078(2) Å is comparable to that of 3.105(2) Å in K_2S_3 [22]. *Ln*–S distances are reasonable and decrease from Nd to Ho in the KLn_2CuS_4 compounds, as expected from the lanthanide contraction.

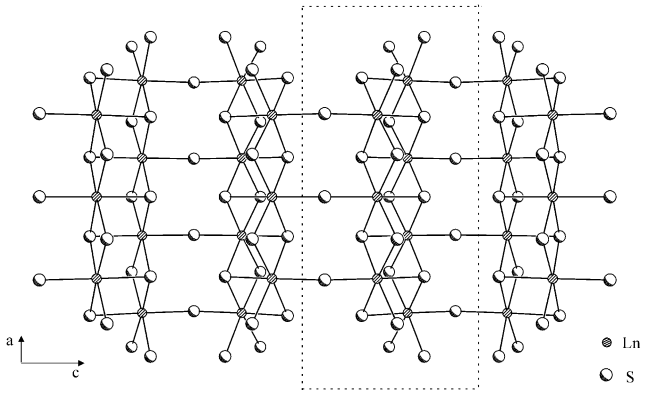

Fig. 5. Structure of the $^2_\infty[Ln_2S_5^{4-}]$ layer in KLn_2CuS_4 viewed down [010]. The $^1_\infty[Ln_2S_6^{6-}]$ chain is in the dashed box.

3.3. Magnetism

A plot of the reciprocal molar susceptibility ($1/\chi$) versus T for $K_2Ho_4Cu_4S_9$ is shown in Fig. 8. $K_2Ho_4Cu_4S_9$ shows Curie–Weiss paramagnetic behavior between 5 and 300 K, with a Curie constant C of 14.33(5) emu K mol^{-1} and a Weiss constant θ_p of −16.5(4) K. The calculated effective magnetic moment of 10.71 μ_B agrees well with the theoretical value of 10.60 μ_B for Ho^{3+} [23].

3.4. Optical properties

The diffuse reflectance spectra of KSm_2CuS_4 and $K_2Ho_4Cu_4S_9$ are shown in Fig. 9. The optical band gaps of 2.17 eV for KSm_2CuS_4 and 2.43 eV for $K_2Ho_4Cu_4S_9$ were deduced with the use of a straightforward extrapolation method [24]. The absorption peaks at about 650 nm in $K_2Ho_4Cu_4S_9$ are typical $4f$–$4f$ optical transitions for Ho^{3+} [25].

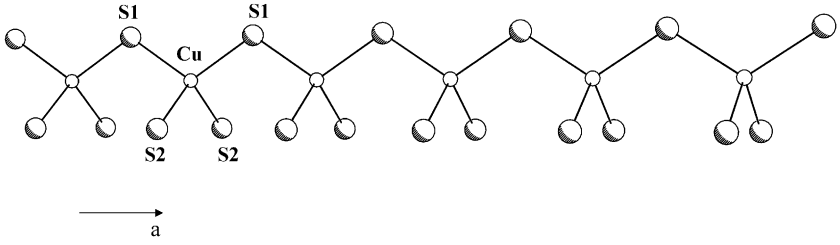

Fig 6. Structure of the $^1_\infty[CuS_3^{5-}]$ chain in KLn_2CuS_4.

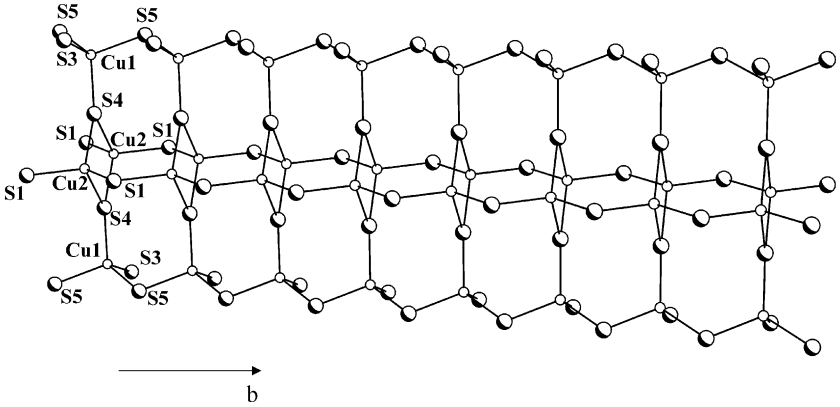

Fig. 7. Structure of the $^1_\infty[Cu_4S_8^{12-}]$ chain in $K_2Ln_4Cu_4S_9$.

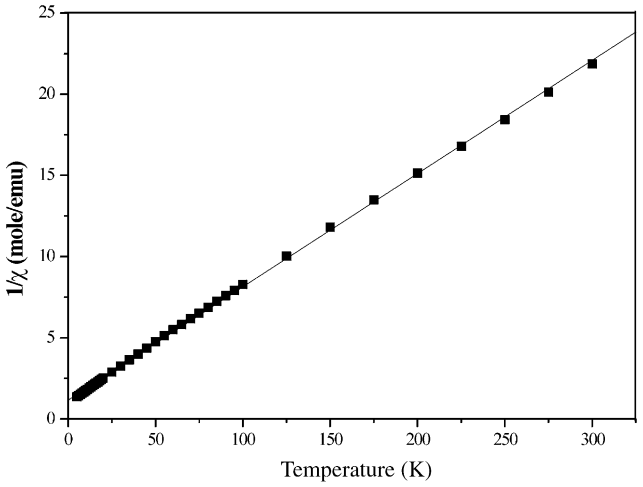

Fig. 8. Plot of the inverse magnetic susceptibility ($1/\chi$) versus T for $K_2Ho_4Cu_4S_9$, where the solid line is the least-squares fit.

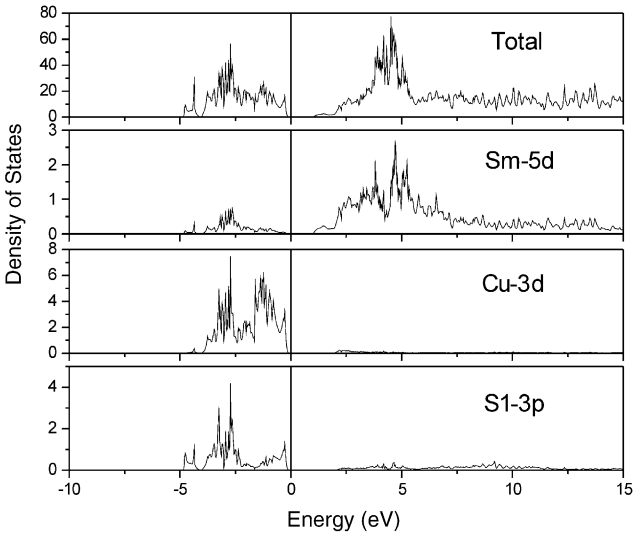

Fig. 10. Density of states (DOS) of KSm_2CuS_4.

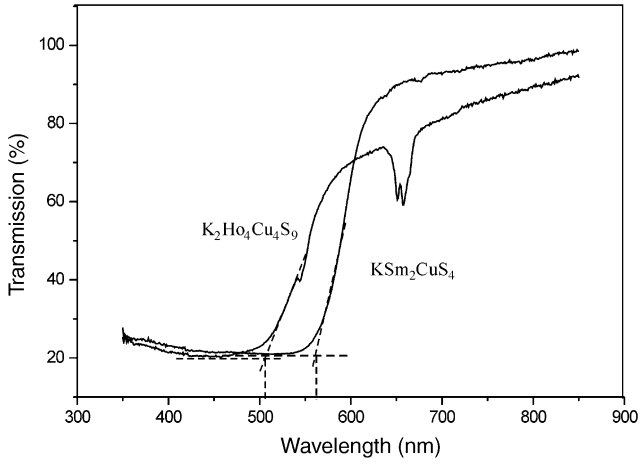

Fig. 9. Diffuse reflectance spectra of KSm_2CuS_4 and $K_2Ho_4Cu_4S_9$.

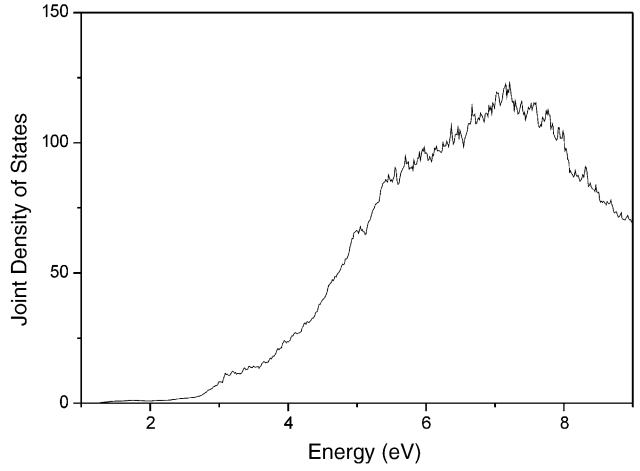

Fig. 11. Joint density of states (JDOS) of KSm_2CuS_4.

3.5. Theoretical calculations

The total and partial density of states (DOS) of KSm_2CuS_4 are shown in Fig. 10. Most of the contributions around the Fermi level are from the 3*p* electrons of S, 3*d* electrons of Cu, and 5*d* electrons of Sm. Since K has almost no contributions in the DOS, the electronic properties are mainly determined by the three-dimensional $[Sm_2CuS_4]^-$ anionic framework. Analysis of the partial DOS shows that the S-3*p* and Cu-3*d* are found mostly in the valence band, whereas the Sm-5*d* lies mainly in the conduction band. The experimental band gap for KSm_2CuS_4 is 2.17 eV but from the total DOS the gap between conduction and valence bands is only about 1.0 eV. Thus, the optical transition is not from the highest occupied molecular orbital (HOMO) to the lowest unoccupied molecular orbital (LUMO). The band structure (not shown) also indicates that the maximum of the valence band and the minimum of the conduction band are not located at the same k point; thus the gap of 1.0 eV is an indirect gap.

Consider the interband transitions, where the occupied valence band states are the initial states and the unoccupied conduction band states are the final states. The JDOS is related to a convolution over the valence band and the conduction band DOS functions. It corresponds to the optical transitions between the valence and conduction band states. The JDOS is zero if the transitions are forbidden or if no initial or final states are present at the transition energy. It is large for allowed transitions between bands with a large DOS at the transition energy. In WIEN2k, the JDOS is calculated by summing over all the allowed interband transitions at the transition energy, weighted by optical matrix elements. Fig. 11 shows the JDOS of KSm_2CuS_4. An optical transition between 2.0 and 2.5 eV can be

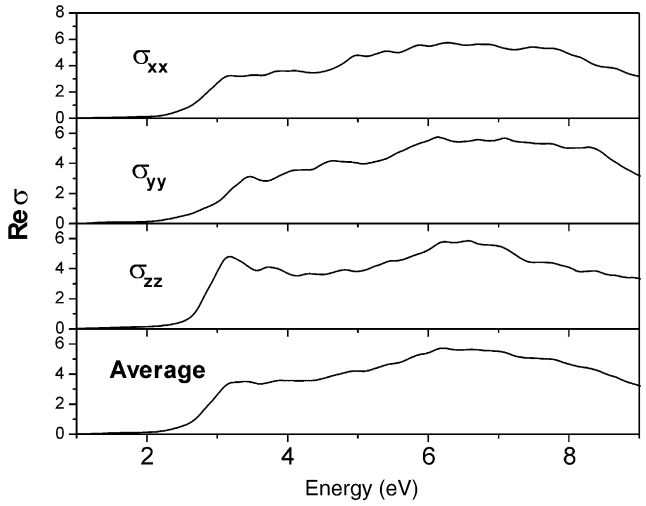

Fig. 12. Real part of the frequency-dependent optical conductivity for KSm_2CuS_4 (in units of 10^{15}/s).

deduced from this figure. For a more accurate value, the real parts of optical conductivity constants were also calculated. The real parts of the optical conductivity components, σ_{xx}, σ_{yy}, and σ_{zz}, are shown in Fig. 12. There is no significant difference in these three optical conductivity tensor components. From the average over these three, a band gap of about 2.1 eV is obtained, in surprisingly good agreement with the experimental value of 2.17 eV.

Acknowledgments

This research was supported by National Science Foundation Grant DMR00-96676 and by the MRSEC Program of the National Science Foundation (DMR00-76097) at the Materials Research Center of Northwestern University.

References

[1] K. Mitchell, J.A. Ibers, Chem. Rev. 102 (2002) 1929–1952.
[2] S.A. Sunshine, D. Kang, J.A. Ibers, J. Am. Chem. Soc. 109 (1987) 6202–6204.
[3] S.A. Sunshine, D.A. Keszler, J.A. Ibers, Acc. Chem. Res. 20 (1987) 395–400.
[4] Bruker, SMART Version 5.054 Data Collection and SAINT-Plus Version 6.22 Data Processing Software for the SMART System, Bruker Analytical X-ray Instruments, Inc., Madison, WI, USA, 2000.
[5] G.M. Sheldrick, SHELXTL DOS/Windows/NT Version 6.12, Bruker Analytical X-ray Instruments, Inc., Madison, WI, USA, 2000.
[6] L.M. Gelato, E. Parthé, J. Appl. Crystallogr. 20 (1987) 139–143.
[7] C.J. O'Connor, Prog. Inorg. Chem. 29 (1982) 203–283.
[8] E. Wimmer, H. Krakauer, M. Weinert, A.J. Freeman, Phys. Rev. B 24 (1981) 864–875.
[9] M. Weinert, E. Wimmer, A.J. Freeman, Phys. Rev. B 26 (1982) 4571–4578.
[10] P. Blaha, K. Schwarz, G. Madsen, D. Kvasnicka, J. Luitz, WIEN2k, 2001.
[11] J.P. Perdew, Y. Wang, Phys. Rev. B: Condens. Matter 45 (1992) 13244–13249.
[12] P.E. Blöchl, O. Jepsen, O.K. Andersen, Phys. Rev. B: Condens. Matter 49 (1994) 16223–16233.
[13] C. Ambrosch-Draxl, J.A. Majewski, P. Vogl, G. Leising, Phys. Rev. B: Condens. Matter 51 (1995) 9668–9676.
[14] T. Nautiyal, S. Auluck, P. Blaha, C. Ambrosch-Draxl, Phys. Rev. B 62 (2000) 15547–15552.
[15] P. Stoll, P. Dürichen, C. Näther, W. Bensch, Z. Anorg. Allg. Chem. 624 (1998) 1807–1810.
[16] F.Q. Huang, J.A. Ibers, J. Solid State Chem. 151 (2000) 317–322.
[17] P. Wu, J.A. Ibers, J. Solid State Chem. 110 (1994) 156–161.
[18] F.Q. Huang, J.A. Ibers, J. Solid State Chem. 158 (2001) 299–306.
[19] Y. Yang, J.A. Ibers, J. Solid State Chem. 149 (2000) 384–390.
[20] A. Meetsma, G.A. Wiegers, R.J. Haange, J.L. de Boer, G. Boom, Acta Crystallogr., Sect. C: Cryst. Struct. Commun. 47 (1991) 2287–2291.
[21] A. van der Lee, R. van de Belt, G.A. Wiegers, J. Alloys Compd. 178 (1992) 57–70.
[22] P. Böttcher, Z. Anorg. Allg. Chem. 432 (1977) 167–172.
[23] C. Kittel, Introduction to Solid State Physics, 6th Edition, Wiley, New York, 1986.
[24] O. Schevciw, W.B. White, Mater. Res. Bull. 18 (1983) 1059–1068.
[25] S. Cotton, Lanthanides and Actinides, Oxford University Press, New York, 1991, p. 29.